

See discussions, stats, and author profiles for this publication at: <https://www.researchgate.net/publication/7431555>

# Two-dimensional Hyperfine Sublevel Correlation Spectroscopy: Powder Features for S=1/2, I=1

ARTICLE in JOURNAL OF MAGNETIC RESONANCE · APRIL 2006

Impact Factor: 2.51 · DOI: 10.1016/j.jmr.2005.11.013 · Source: PubMed

---

CITATIONS

10

READS

16

## 2 AUTHORS, INCLUDING:



Michael K. Bowman  
University of Alabama

179 PUBLICATIONS 3,836 CITATIONS

[SEE PROFILE](#)



Available online at www.sciencedirect.com



Journal of Magnetic Resonance xxx (2005) xxx–xxx

**JMR**  
Journal of  
Magnetic Resonance

www.elsevier.com/locate/jmr

## Two-dimensional hyperfine sublevel correlation spectroscopy: Powder features for $S = 1/2, I = 1$

Alexander G. Maryasov <sup>a,b,\*</sup>, Michael K. Bowman <sup>b</sup><sup>a</sup> Institute of Chemical Kinetics and Combustion, Siberian Branch of Russian Academy of Sciences, Novosibirsk 630090, Russian Federation<sup>b</sup> Structural Biology and Microimaging, Battelle Northwest, Richland, WA 99354, USA

Received 26 August 2005; revised 20 November 2005

### Abstract

The lineshapes of two-dimensional magnetic resonance spectra of disordered or partially ordered solids are dominated by ridges of singularities in the frequency plane. The positions of these ridges are described by a branch of mathematics known as catastrophe theory concerning the mapping of one 2D surface onto another. We systematically consider the characteristics of HYScore spectra for paramagnetic centers having electron spin  $S = 1/2$  and nuclear spin  $I = 1$  in terms of singularities using an exact solution of the nuclear spin Hamiltonian. The lineshape characteristics are considered for several general cases: zero nuclear quadrupole coupling; isotropic hyperfine but arbitrary nuclear quadrupole couplings; coincident principal axes for the nuclear hyperfine and quadrupole tensors; and the general case of arbitrary nuclear quadrupole and hyperfine tensors. The patterns of singularities in the HYScore spectra are described for each case.

© 2005 Published by Elsevier Inc.

**Keywords:** ESE EM; HYScore; 2D spectroscopy; Catastrophe theory; Nitrogen nucleus; Hyperfine interaction; Singularity patterns; Mapping; Quadrupolar interaction; Fold; Cusp

### 1. Introduction

Techniques to allow observation of multidimensional spectra are widely applied in magnetic resonance spectroscopy for better resolution and easier interpretation of experimental data [1,2]. Two-dimensional (2D) displays of spectra are used extensively because they are readily visualized. In both electron paramagnetic resonance and nuclear magnetic resonance (EPR and NMR) spectroscopies, 2D spectra are obtained as slices or projections of higher dimensional spectra or by applying some pulse sequence to the system in question where two time intervals,  $t_1$  and  $t_2$ , in the pulse sequence are varied independently, see Fig. 1. The system response (typically spin echo or free induction signal) is stored as a 2D array of data. After 2D Fourier transformation, one obtains the

2D spectral density of the signal in the  $\omega_1, \omega_2$  plane, where the frequency,  $\omega_j$ , is the Fourier conjugate of  $t_j$ . In solid state measurements, such spectra often have complicated lineshapes because of anisotropic interactions that cause molecules with different orientations to have different spectral frequencies. If the molecules in the sample have complete or partial orientational disorder, (often referred to as ‘powder’ samples), the detailed lineshapes offer an opportunity to determine the complete, anisotropic magnetic resonance parameters of the molecule (see, e.g. [3,4]).

In 2D Fourier magnetic resonance experiments, the time-domain signal produced by molecules at any single, arbitrary orientation may be presented as

$$V(t_1, t_2) = \sum_{j,k=1}^N A_{j,k} \exp(i\Omega_j t_1 + i\Omega_k t_2), \quad (1)$$

where the frequencies  $\Omega_j$  depend on the spin Hamiltonian eigenvalues and in simple cases are the transition frequencies of the system. The amplitudes,  $A_{j,k}$ , depend on the

\* Corresponding author. Fax: +7 383 330 7350.

E-mail address: maryasov@ns.kinetics.nsc.ru (A.G. Maryasov).

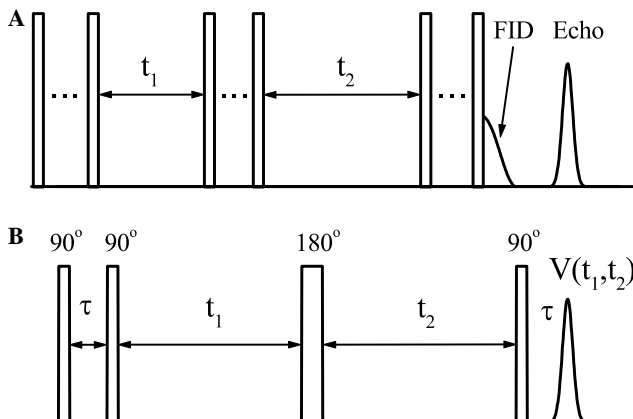


Fig. 1. Pulse sequences used in two-dimensional spectroscopy, (A) the general scheme, and (B) HYSCORE experiment implementation. In the latter case the stimulated echo signal amplitude is measured. It is generated by the first, second and the fourth pulses. The signal amplitude is measured as a function of two delays,  $t_1$  and  $t_2$ , between the mixing (third) pulse and second and fourth pulses, respectively. The rotation angles are shown above the pulses.

characteristics of the microwave (mw) pulses in the case of EPR or radiofrequency (rf) pulses in the case of NMR, the particular pulse sequence, and on the parameters of the spin Hamiltonian. Both  $\Omega_j$  and  $A_{j,k}$  implicitly depend on the orientation of the molecule in the magnetic field of the spectrometer because the spin Hamiltonian generally is orientation dependent. In this paper, we use a type of 2D EPR spectroscopy known as HYSCORE [7] as a specific example, although the approach is applicable to other types of 2D EPR [8–10] or NMR methods. For simplicity, we do not consider relaxation in Eq. (1) and assume both frequencies to be non-zero. In general, the signal described by Eq. (1) consists of damped periodic oscillations in the time domain. We ignore the damping here because it is usually negligible compared to damping caused by interference from the distribution of frequencies in a ‘powder’ sample.

Fourier transformation of Eq. (1) gives

$$V_F(\omega_1, \omega_2) = \sum_{j,k=1}^N A_{j,k} \delta(\omega_1 - \Omega_j) \delta(\omega_2 - \Omega_k), \quad (2)$$

where  $\delta(x)$  is Dirac’s delta-function. Instead of a smooth function of two variables in the time domain, the transformed signal is a set of discrete points in the frequency domain having infinite amplitude and zero spectral density in the rest of the frequency plane. For an orientationally disordered or ‘powder’ sample, Eqs. (1) and (2) must be integrated over the orientations of the molecules in the sample with respect to the laboratory frame. Such integration leads to a set of regions or spectral ‘lines’ having non-zero spectral density, which may partly overlap each other. The boundaries between regions with zero and non-zero spectral density often form rather prominent ridges. Such 2D patterns of ridges allow precise determination of the spin Hamiltonian parameters from which valid inferences of the molecular or electronic structure can be made and is

the motivation for the use of ‘contour lineshapes’ developed by Dikanov [5]. In favorable cases, spin Hamiltonian parameters are determined completely by the positions of the ridges without the need to consider the intensity factors in Eqs. (1) and (2). This paper systematically examines the shapes of these ridges and the question of whether prominent ridges lie only on the boundaries between regions with and without spectral density.

From the point of view of mathematics, each term in Eq. (2) represents a smooth mapping of the hemisphere of possible orientations onto the frequency plane

$$\begin{cases} \omega_1 = \Omega_j(\theta, \phi) \\ \omega_2 = \Omega_k(\theta, \phi) \end{cases}. \quad (3)$$

Here  $\theta$  and  $\phi$  are the polar and azimuthal angles relating the external magnetic field to the molecular frame. Because inversion of the magnetic field does not change the eigenvalues of the spin-Hamiltonian, only a hemisphere of possible orientations need be considered. We will make extensive use of the unit hemisphere defined by  $\theta$  and  $\phi$  in discussing the orientation dependence of the spectral frequencies in the 2D spectra. This smooth mapping generates singularities where many orientations of a paramagnetic center (PC) result in the same set of frequencies so that significant areas of the hemisphere map to a single, intense point in the frequency plane.

These singularities produce a 2D ‘powder’ spectrum with prominent features where the signal intensity approaches infinity in the ideal case. The branch of mathematics which concerns singularities in the smooth mappings of one metric space onto the other is called catastrophe theory [6]. We used catastrophe theory to predict and understand features in HYSCORE spectra for different classes of spin Hamiltonians but for this paper we try to explain those results with more familiar mathematics. Other approaches have been used with great success (see the excellent discussion of 2D NMR powder lineshapes in [S-R & S]).

In HYSCORE spectra, the singularities are modified by the intensity factor,  $A_{j,k}$ . The intensity factor is strictly bounded, generally,  $0 \leq |A_{j,k}|^2 \leq 1$ . These intensity factors may cause part of a singularity to have zero amplitude, but they can never produce a singularity independent of the mapping. Thus, the prominent features in a spectrum correspond to singularities whose locations can be determined without calculating the  $A_{j,k}$  although not every singularity will have sufficient intensity to be observed.

This paper considers 2D spectroscopy in ‘powder’ samples in the context of catastrophe theory and focuses on the features of the spectrum that arise from singularities produced by the mapping because in many cases the locations of these singularities are sufficient to determine the desired spin Hamiltonian parameters. A form of 2D pulsed EPR spectroscopy, known as hyperfine sublevel correlation (HYSCORE) spectroscopy [7], of PCs having electron spin  $S = 1/2$  and nuclear spin  $I = 1$  is used as a specific spectroscopic example. HYSCORE uses the electron spin for the

146 indirect detection of nuclear spin coherences generated in  
 147 nuclei with an appreciable hyperfine coupling to the PC.

148 Our analysis is based on exact solutions of the complete  
 149 nuclear spin Hamiltonians. Although the discussion is in  
 150 the context of HYSCORE spectroscopy, it is directly relevant  
 151 to other forms of pulsed EPR spectroscopy, for example, 2D TRIPLE [8,9], 2D ENDOR ESEEM correlation  
 153 spectroscopy [8] or double nuclear coherence transfer  
 154 (DONUT)-HYSCORE spectroscopy [10]. Catastrophe theory  
 155 has been used in the theory of nonlinear resonances in  
 156 molecular spectroscopy (see, e.g. [11]) and in ferromagnetic  
 157 resonance spectra [12].

158 The origin of the nuclear quantum beats in pulsed EPR  
 159 experiments such as HYSCORE will be outlined first, fol-  
 160 lowed by a few important results from catastrophe theory  
 161 relevant to this paper. Then the 2D ‘powder’ lineshapes  
 162 in HYSCORE spectra will be considered for several general  
 163 classes of spin Hamiltonians. Although numerical simula-  
 164 tions of HYSCORE spectra have been made for specific  
 165 sets of spin Hamiltonian parameters and analytical results  
 166 obtained for the simpler cases, this is the first systematic  
 167 investigation of the locations of the singularities and the  
 168 methods to rapidly calculate their locations.

## 169 2. Electron spin echo envelope modulation and HYSCORE 170 spectra

171 The effect of electron spin echo (ESE) envelope modula-  
 172 tion (EM) [13,14] was discovered about four decades ago  
 173 and is a periodic oscillation in the electron spin echo signal  
 174 amplitude as the time interval between microwave pulses is  
 175 varied. Electron spin flips produced by nonselective mw  
 176 pulses change the local magnetic field produced by the  
 177 hyperfine interaction (hfi) at a nearby nucleus. These  
 178 instantaneous changes in local field generate interfering  
 179 nuclear coherences or, in other words, quantum beats in  
 180 the nuclear subsystem. These quantum beats give rise in  
 181 ESE experiments to an amplitude modulation of the echo  
 182 known as EM.

183 Let us consider the EM in detail using a vector model we  
 184 originally defined for the case of  $S = 1/2$ ,  $I = 1/2$  and  
 185 which we now extend to  $S = 1/2$ ,  $I = 1$ . The system Ham-  
 186 iltonian (in units of angular frequency) consists of three  
 187 terms

$$188 \hat{H} = \hat{H}_S + \hat{\vec{S}} \cdot \hat{\vec{A}} \hat{\vec{I}} + \hat{H}_I, \quad (4)$$

189 where the first and the third terms depend on the electron  
 190 and nuclear spin operators, respectively, and the second  
 191 term describes the electron—nuclear hfi with  $\vec{A}$  being the  
 192 tensor of this interaction. In the case of (effective) electron  
 193 spin,  $S = 1/2$ ,  $H_S$  reduces to the electron Zeeman interac-  
 194 tion. In many cases, the quantization axis for the electron  
 195 spin coincides with the direction of the external magnetic  
 196 field  $\vec{k}_z$  (this direction is chosen as the  $z$  axis of the labora-  
 197 tory frame) with high accuracy so the first and the second  
 198 terms in the Hamiltonian (4) may be written in the form

$$\hat{H}_S + \hat{\vec{S}} \cdot \hat{\vec{A}} \hat{\vec{I}} \approx \omega_S \hat{S}_z + \hat{S}_z (\vec{A} \cdot \hat{\vec{I}}) \quad (5)$$

199 for the typical ‘high field’ limit in which  $|\hat{H}_S| \gg |\hat{\vec{S}} \cdot \hat{\vec{A}} \hat{\vec{I}}|, |\hat{H}_I|$ . Here the vector  $\vec{A}$  is proportional to the hyperfine field pro-  
 200 duced at the nucleus by the electron spin

$$\vec{A} = \vec{k}_z \hat{\vec{A}}. \quad (6)$$

201 The approximation (5) allows factorization of the system  
 202 eigenfunctions as a product of wavefunctions,  $|\psi\rangle =$   
 $|m_S\rangle |\psi_{I,m_S}\rangle$ , where the second term in the product is the  
 203 eigenfunction of the nuclear subhamiltonian,  $\hat{H}_{I,m_S}$ , corre-  
 204 sponding to a manifold of states with  $m_S$  being the projec-  
 205 tion of the electron spin onto its quantization axis, in our  
 206 case  $m_S = \pm 1/2$ . This operator may be written as

$$\hat{H}_{I,m_S} = m_S \vec{A} \cdot \hat{\vec{I}} + \hat{H}_I = \omega_I \hat{I}_z + m_S \vec{A} \cdot \hat{\vec{I}} + \hat{\vec{I}} \hat{\vec{Q}} \hat{\vec{I}}. \quad (7)$$

207 Here  $\omega_I$  is the nuclear Zeeman frequency and  $\hat{\vec{Q}}$  is the  
 208 nuclear quadrupolar interaction tensor. Electron spin flips  
 209 induced by mw pulses change the value of  $m_S$  in Eq. (7) and  
 210 can project eigenstates of  $\hat{H}_{I,1/2}$ , for example, into a coherent  
 211 superposition of eigenstates of  $\hat{H}_{I,-1/2}$ , giving rise to the  
 212 quantum beats.

213 For spin  $I = 1$ , the Hamiltonian (7) was solved in a series  
 214 of papers by Muha [15] in trigonometric form. The  
 215 eigenvalues may be written as

$$\Omega_{m_S,j} = \left( \frac{4|p_{m_S}|}{3} \right)^{1/2} \cos \left[ \frac{\lambda_{m_S} + 2\pi j}{3} \right] \quad (8)$$

216 for  $j = 0, 1, 2$  and

$$\cos \lambda_{m_S} = \frac{q_{m_S}}{2} \left( \frac{3}{|p_{m_S}|} \right)^{3/2}, \quad (9)$$

217 where (see also our earlier paper [16])

$$p_{m_S} = -[D_{m_S}^2 + \kappa^2(3 + \eta^2)], \quad (10)$$

$$q_{m_S} = \vec{D}_{m_S} \hat{\vec{Q}} \vec{D}_{m_S} - 2\kappa^3(1 - \eta^2). \quad (11)$$

218 Here  $\vec{D}_{m_S}$  is the effective field (in units of an angular fre-  
 219 quency) affecting the nuclear spin, given by the vector sum  
 220 of the external magnetic field and the hyperfine field

$$\vec{D}_{m_S} = \omega_I \vec{k}_z + m_S \vec{A} \quad (12)$$

223 and  $D_{m_S}$  is its length. The nuclear quadrupole interaction  
 224 tensor is often written as

$$\hat{\vec{Q}} = \begin{bmatrix} -(1-\eta)\kappa & 0 & 0 \\ 0 & -(1+\eta)\kappa & 0 \\ 0 & 0 & 2\kappa \end{bmatrix} \quad (13)$$

225 in the frame of its principal axes, here  $\kappa$  is the quadrupolar  
 226 coupling constant, and  $\eta$  is the asymmetry parameter.

227 The four pulse sequence producing the HYSCORE  
 228 spectra is shown in Fig. 1B. The measured signal is the  
 229 stimulated echo amplitude generated by the 1st, 2nd, and  
 230 4th pulses as a function of the two delays  $t_1$  (between the  
 231 2nd and the 3rd inverting pulse) and  $t_2$  (between the 3rd  
 232 and the 4th inverting pulse).

and the 4th pulses) as shown in the figure. In this case, the 2D spectral density given by Eq. (2) for a PC having a particular orientation may be written as

$$V_F(\omega_1, \omega_2) = \sum_{n,j,r,s} \delta(\omega_1 - \Omega_\alpha^{j,n}) \delta(\omega_2 - \Omega_\beta^{r,s}) A_{njrs}(\theta, \phi) \\ + \sum_{n,j,r,s} \delta(\omega_1 - \Omega_\beta^{j,n}) \delta(\omega_2 - \Omega_\alpha^{r,s}) B_{njrs}(\theta, \phi), \quad (14)$$

where the transition frequencies of the nuclear subhamiltonians are [15,16]

$$\Omega_{ms}^{j,k} = \Omega_{ms,j} - \Omega_{ms,k} = 2|p_{ms}|^{1/2} \operatorname{sgn}[k-j] \xi_{ms,j+k} \quad (15)$$

with

$$\xi_{ms,n} = \sin \left[ \frac{\lambda_{ms} + \pi n}{3} \right] \quad (16)$$

being a dimensionless factor,  $\alpha$  and  $\beta$  are used here and below instead of  $m_s = +1/2$  and  $m_s = -1/2$ , respectively, for better readability. The number  $n$  ( $n = 1, 2, 3$ ) in Eq. (16) indexes the three possible transitions in the spectrum of the nucleus [15,16]. The largest transition frequency occurs for  $n = 1$  and is often called the double quantum (dq) transition while the  $n = 2$  and 3 transitions are called single quantum (sq) transitions. The amplitudes  $A$  and  $B$  may be calculated in the framework of the standard description of HYSCORE [2,5] using the Mims matrices [17],  $M$ , whose elements are scalar products of nuclear eigenfunctions belonging to different electron spin manifolds, or using the spectral decomposition of subhamiltonians from Eq. (7) as developed in [16]. In the latter case, only the eigenvalues are needed for the calculations. In this paper, the explicit forms of the amplitudes are of no importance, only the fact that their magnitude is less than unity.

Each product of delta-functions in Eq. (14) maps the hemisphere of orientations onto the frequency plane. Each product correlates transition frequencies from two different electron spin manifolds, providing an opportunity to extract the parameters of the nuclear subhamiltonians. There are 72 terms in Eq. (14) for  $I = 1$  that map onto 72 distinct but often overlapping regions of the entire frequency plane. Each term maps the unit hemisphere into a single, continuous region whose outline is a singularity. Because of the symmetry of the HYSCORE spectra [2] usually only the  $\omega_2 \geq 0$  half-plane with 36 ridges is displayed.

Let us consider one term from Eq. (14), for example, the one with the coefficient  $A_{njrs}$ . The appropriate mapping will be:

$$\omega_1 = \Omega_\alpha^{j,n}(\theta, \phi), \\ \omega_2 = \Omega_\beta^{r,s}(\theta, \phi). \quad (17)$$

The singularities produced by this mapping provide the region with fine structure consisting of one or a few ridges where the spectral density goes to infinity. Any ridge may cross itself or another ridge from the same or a different region. In Section 4, we consider in detail the patterns that

these ridges form for several general types of nuclear spin Hamiltonians. 314  
315

### 3. Relevant results from catastrophe theory

Eq. (17) describes a smooth mapping (since  $\omega_1$  and  $\omega_2$  are functions of  $\theta$  and  $\phi$ )  $R_2 \Rightarrow R_2$ , where  $R_i$  is an  $i$ -dimensional metric space. All possible singularities resulting from such a mapping in the general case were described in the paper by Whitney half-a-century ago [18]. The theory of singularities of smooth mappings of multidimensional spaces forms a part of catastrophe theory together with the theories of caustics of wave fronts and bifurcations of solutions of ordinary nonlinear differential equations [6], where similar objects appear.

For us, the most important result is the discovery by Whitney [18] that, in the general case, only two types of singularities exist. Whitney called these folds and cusps, see Fig. 2 for examples. An example of a fold is the projection of a sphere onto a plane. Each point on the plane near the fold singularity corresponds to zero or two points on the surface of the sphere. The case of a cusp is less simple; it may be described as the junction of two annihilating folds. Near a cusp, each point on most of the plane corresponds to only one point of the projected surface while inside a narrow angle each point on the plane corresponds to three points on the projected surface with fold singularities meeting at a cusp separating these regions of the plane. More complex singularities are special cases that may be reduced to a set of folds and cusps by arbitrarily small distortions of the projected surface bringing it into a condition known as a “general position.” The singularity that forms the outline of a spectral region cannot contain a cusp because there must be at least one point of the surface on either side of a cusp while no point on the unit hemisphere can be projected outside the spectral region. This means that any cusps that exist must lie in the interior of the HYSCORE line.

The singularities in the mapping (17) obey a simple equation obtained from catastrophe theory or the calculus of coordinate transformations [4]. That is, the Jacobian,  $J$ , of the mapping vanishes on these lines

$$J = \frac{\partial (\Omega_\alpha^{j,n}(\theta, \phi), \Omega_\beta^{r,s}(\theta, \phi))}{\partial (\theta, \phi)} \\ = \frac{\partial \Omega_\alpha^{j,n}}{\partial \theta} \frac{\partial \Omega_\beta^{r,s}}{\partial \phi} - \frac{\partial \Omega_\alpha^{j,n}}{\partial \phi} \frac{\partial \Omega_\beta^{r,s}}{\partial \theta} = 0. \quad (18)$$

Relation (18) may be rewritten in an equivalent and rather compact form, as discovered in 2D NMR spectroscopy [3]

$$\vec{\nabla} \Omega_\alpha^{j,n} \times \vec{\nabla} \Omega_\beta^{r,s} = 0. \quad (19)$$

Here Hamilton's nabla operator,  $\vec{\nabla}$ , is used for the gradient calculations.

Each transition frequency in Eq. (19) depends on  $p_{ms}$  and  $q_{ms}$  from Eqs. (10) and (11), respectively, so that one can rewrite the Jacobian (18) as

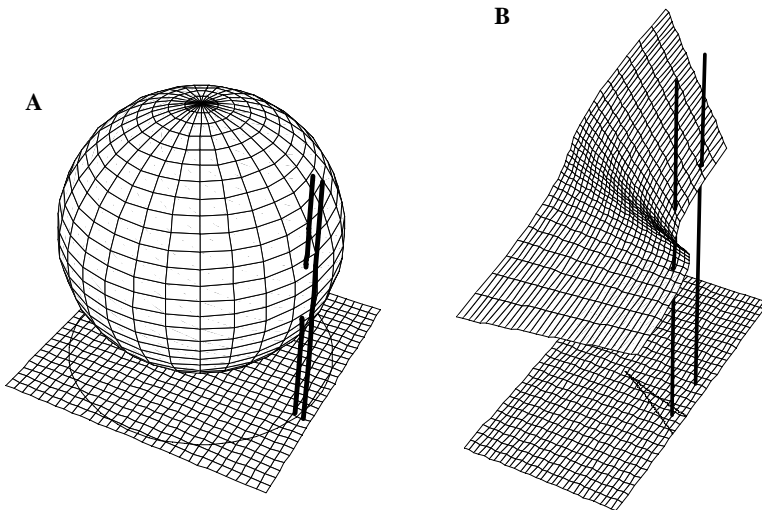


Fig. 2. The two general types of singularities in a smooth mapping  $R_2 \Rightarrow R_2$  according to Whitney, (A) a fold which occurs along the circle formed when a sphere is projected onto a plane, and (B) a cusp located at the apex of the triangular figure on the plane. The vertical lines illustrate that (A) points on the plane on opposite sides of the fold correspond to two points of the sphere (the left line crosses the sphere two times) or no points of the sphere (the right line does not cross the sphere); and (B) the number of points projected onto the plane is 3 inside the cusp (the left line crosses the surface three times) and just one outside it (the right line crosses the surface at one point).

366

$$J = \frac{\partial \Omega_x}{\partial p_x} \frac{\partial \Omega_\beta}{\partial p_\beta} \frac{\partial(p_x, p_\beta)}{\partial(\theta, \phi)} + \frac{\partial \Omega_x}{\partial p_x} \frac{\partial \Omega_\beta}{\partial q_\beta} \frac{\partial(p_x, q_\beta)}{\partial(\theta, \phi)} + \frac{\partial \Omega_x}{\partial q_x} \\ \times \frac{\partial \Omega_\beta}{\partial p_\beta} \frac{\partial(q_x, p_\beta)}{\partial(\theta, \phi)} + \frac{\partial \Omega_x}{\partial q_x} \frac{\partial \Omega_\beta}{\partial q_\beta} \frac{\partial(q_x, q_\beta)}{\partial(\theta, \phi)}. \quad (20)$$

368 Here the upper indices are omitted for simplicity. The partial derivatives of the transition frequencies in the above equation may be calculated easily using Eq. (15):

$$\frac{\partial \Omega_{ms}^{j,k}}{\partial p_{ms}} = \frac{\Omega_{ms}^{j,k}}{2p_{ms}} + 2\text{sgn}[k-j]|p_{ms}|^{1/2} \frac{\partial \xi_{ms,j+k}}{\partial p_{ms}}, \quad (21)$$

$$\frac{\partial \Omega_{ms}^{j,k}}{\partial q_{ms}} = 2\text{sgn}[k-j]|p_{ms}|^{1/2} \frac{\partial \xi_{ms,j+k}}{\partial q_{ms}}. \quad (22)$$

378 With the help of Eq. (16) one can obtain

$$\frac{\partial \xi_{ms,n}}{\partial u_{ms}} = \frac{1}{3} \cos \left[ \frac{\lambda_{ms} + \pi n}{3} \right] \frac{\partial \lambda_{ms}}{\partial u_{ms}}, \quad (23)$$

382 where  $u$  represents  $p$  and  $q$  as needed. The derivatives of  $\lambda$  may be calculated using its definition in Eq. (9):

$$\frac{\partial \lambda_{ms}}{\partial p_{ms}} = \frac{3 \cos \lambda_{ms}}{2p_{ms} \sin \lambda_{ms}}, \quad (24)$$

$$\frac{\partial \lambda_{ms}}{\partial q_{ms}} = -\frac{\cos \lambda_{ms}}{q_{ms} \sin \lambda_{ms}}. \quad (25)$$

390 Taking account of Eqs. (8) and (23)–(25) one can rewrite Eqs. (21) and (22) as:

$$\frac{\partial \Omega_{ms}^{j,k}}{\partial p_{ms}} = \frac{\Omega_{ms}^{j,k}}{2p_{ms}} + \frac{\sqrt{3}\text{sgn}[k-j]\cos \lambda_{ms}}{4 \cos \left[ \frac{\pi(k-j)}{3} \right]} \frac{\Omega_{ms,j} + \Omega_{ms,k}}{p_{ms}}, \quad (26)$$

$$\frac{\partial \Omega_{ms}^{j,k}}{\partial q_{ms}} = -\frac{\text{sgn}[k-j]\cos \lambda_{ms}}{2\sqrt{3} \cos \left[ \frac{\pi(k-j)}{3} \right]} \frac{\Omega_{ms,j} + \Omega_{ms,k}}{q_{ms}}. \quad (27)$$

It is clear that the location of the singularities in the frequency plane can be found by classic mathematical analysis without recourse to catastrophe theory. However, catastrophe theory does allow us to recognize and categorize the types of singularities that do occur. In addition, the ridges of singularities in a spectrum can be quickly visualized with minimal computational effort using another branch of catastrophe theory: the caustics of wave fronts or singularities of the system of rays. When wave fronts, for instance, those of light, propagate through inhomogeneous media, these waves may have high relative amplitude in places because of constructive interference of these waves. That is, at singularities of the wave fronts. Wave front propagation can also be posed in terms of the propagation of rays which are normal to the surface of the wave front. Such a system of rays also may have caustics (singularities) where they are focused by the medium.

On the unit hemisphere, the parallels or lines of latitude start from the pole and expand in a set of concentric circles out to the equator while the meridians or lines of longitude radiate out from the poles, and are everywhere perpendicular to the parallels. These parallels and meridians behave like wavefronts and rays, respectively. The mapping of the unit hemisphere onto the frequency plane by Eq. (17) behaves like the propagation of rays and wavefronts through anisotropic media. The singularities of the mapping occur where rays or wavefronts pile up on top of each other. The prominent singularities in a HYSCORE line-shape can be quickly identified with little computational effort by seeing where the parallels and meridians pile up when they are mapped onto the frequency plane as illustrated later.

Many of our conclusions are based on the mapping of a closed surface onto the frequency plane. Yet the unit hemisphere is not a closed surface and might be expected to

396  
397  
398  
399  
400  
401  
402  
403  
404  
405  
406  
407  
408  
409  
410  
411  
412  
413  
414  
415  
416  
417  
418  
419  
420  
421  
422  
423  
424  
425  
426  
427  
428  
429  
430

have an open ‘edge’ or boundary. But for magnetic resonance, the unit hemisphere has no bounds from the point of view of topology because of the inversion symmetry of the spin Hamiltonian. The eigenvalues are invariant with respect to inversion of the external magnetic field  $\vec{k}_z \Rightarrow -\vec{k}_z$ , producing an interesting topological property. The equator of any arbitrary hemisphere is mapped onto the frequency plane twice because the frequencies of opposite points on the sphere coincide. This means that, one can think of the opposite points on the equator as ‘glued’ together, see Fig. 3, to make the unit hemisphere behave in the context of mapping as if it had no edges. The frequencies change smoothly as one jumps to the opposite point at the equator. Let us underline that the final step after the twofold folding in Fig. 3D is to glue the layers in pairs: the first (counting from top to bottom) with the third, the second with the fourth, this stage is not shown in the figure. Such a glued hemisphere will have self-crossing surfaces. This feature results in rather complex singularity patterns in the general case of the nuclear subhamiltonian having no symmetry and will be illustrated later.

#### 4. HYSCORE spectra in several important cases

We now consider a few general cases of HYSCORE spectra with electron spin  $S = 1/2$  and nuclear spin  $I = 1$ . We discuss some particular cases where special sets of Hamiltonian parameters are imposed by molecular or crystal symmetry. In the most general case, the nuclear subhamiltonian involves nine independent parameters: the nuclear Zeeman frequency,  $\omega_J$ ; the three principal values of the anisotropic hyperfine tensor,  $A_{U,U}$  (here  $U$  denotes the principal axis direction,  $U = X, Y, Z$ ); the nuclear quad-

rupolar interaction characterized by its strength  $\kappa$  and asymmetry  $\eta$ ; and the three Eulerian angles relating the orientation of the principal axes of NQI tensor to the hfi tensor. This number may be reduced to 8 if the frequency parameters are scaled, e.g., by the nuclear Zeeman frequency. We will comment in Section 5 on the effect of g-factor anisotropy. However, molecular or crystal symmetry may reduce the number of parameters still further, for instance, by making the hyperfine interaction isotropic or the nuclear quadrupole interaction axial.

Catastrophe theory usually deals with the systems of “general position” as explained above. The “general position” situation means that the values of all parameters are not in some way “special,” e.g., degeneracy in the energy levels is not allowed. However, in this section we shall consider cases when the nuclear subhamiltonian has non-accidental degeneracies or symmetry so the “general position” condition is not met. In such cases, we will not break the degeneracy or symmetry as usually done in applications of Catastrophe Theory by an arbitrarily small adjustment to the nuclear spin Hamiltonian. Rather, Catastrophe Theory guides us in reducing the angular space that we map so that the degeneracy is removed and we are in a “general position.” For example we might map a single octant with a specially chosen orientation instead of mapping the entire hemisphere with an arbitrarily chosen pole and be confident that we have not missed any spectral features.

##### 4.1. Absence of NQI

When the quadrupolar interaction is absent, the three eigenvalues of the nuclear subhamiltonian in each electron spin manifold become equidistant. Due to the coincidence of two transition frequencies the total number of unique

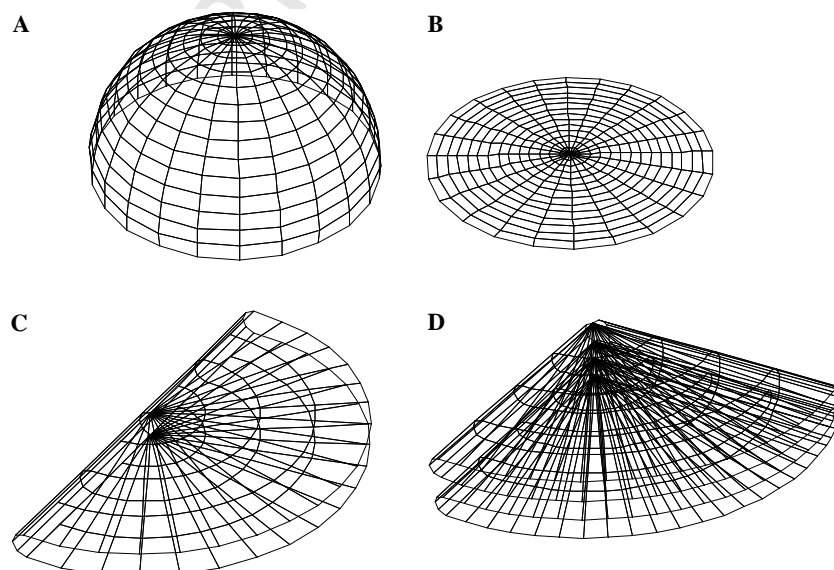


Fig. 3. The topology of the hemisphere due to the symmetry with respect to the inversion. The hemisphere with arbitrary chosen pole as is (A), the hemisphere smoothed out on a plane (B), once (C), and twice (D) folded. After the latter procedure the edges should be glued, the first with the third, and the second with the forth, joining the points where the eigenfrequencies of the nuclear Hamiltonian are the same.

ridges is 16 (in the upper half of the frequency plane) instead of 36 in the general case. The form of the ridges resembles that for nuclear spin  $I = 1/2$  discussed in [5]. Here we consider the specific details for spin  $I = 1$ , giving the Catastrophe Theory results a more conventional explanation.

#### 4.1.1. General case of an anisotropic hyperfine interaction

When the NQI is negligible, the eigenvalues of the nuclear subhamiltonians and respective transition frequencies are easily calculated and the mapping (17) of the singularities onto the frequency plane is simple. The nuclear transition frequencies in this case are calculated from a simplified Eq. (15)

$$Q_{m_S}^{j,k} = c_{j,k} D_{m_S}, \quad (28)$$

where  $c_{j,k}$  is a constant

$$c_{j,k} = 2 \operatorname{sgn}(k-j) \sin \left\{ \frac{\pi}{6} [1 + 2(j+k)] \right\} \quad (29)$$

and  $D_{m_S}$ , Eq. (12), is the strength (in units of angular frequency) of the effective magnetic field affecting the nucleus in the  $m_S$  electron spin manifold,

$$D_{m_S}^2 = \omega_I^2 + \frac{1}{4} \vec{k}_z \overset{\leftrightarrow}{A} \vec{k}_z + m_S \omega_I \vec{k}_z (\overset{\leftrightarrow}{A} \overset{\leftrightarrow}{A}) \vec{k}_z. \quad (30)$$

Here the superscript T denotes the transpose of a matrix. It is clear that  $|c_{j,k}| = 2$  for double quantum (dq) nuclear transitions (when  $j+k=1$ ) or 1 for the single quantum (sq) transitions (when  $j+k>1$ ). In the principal axis system of the hfi tensor Eq. (30) may be presented as

$$D_{m_S}^2 = D_{m_S, X}^2 \sin^2 \theta \cos^2 \phi + D_{m_S, Y}^2 \sin^2 \theta \sin^2 \phi + D_{m_S, Z}^2 \cos^2 \theta. \quad (31)$$

Here  $D_{m_S, U}$  is the length of the vector  $\vec{D}_{m_S}$  when the external magnetic field is directed along  $U$ -th principal axis of the hfi tensor ( $U = X, Y, Z$ )

$$D_{m_S, U}^2 = \omega_I^2 + \frac{1}{4} A_{U, U}^2 + 2m_S \omega_I A_{U, U} \quad (32)$$

with  $A_{U, U}$  being a principal value of the hfi tensor. First we consider the case when all these values are different. Axial symmetry of the hfi tensor is considered below as a special case.

In the absence of NQI, additional symmetry features appear in the mapping (17). The substitutions  $\phi \Rightarrow 2\pi - \phi$  and  $\phi \Rightarrow \pi \pm \phi$  (in the system of hfi tensor) lead to the same transition frequencies (28). It means that the hemisphere is mapped four times onto the same ridges in the frequency plane and that the mappings of its four octants coincide. In this case the hemisphere (for the sake of discussion, the upper one, where  $\cos\theta \geq 0$ ) is folded in half twice, causing pairs of folds to coincide. Such degeneracy violates the “general position” situation considered by catastrophe theory. To resolve this situation, we cut one octant out of the whole sphere first along the edges  $\phi = 0$  and  $\phi = \pi/2$ , and then along the equator where  $\theta = \pi/2$

(see Fig. 3, giving one of the four layers in D). The ‘edges’ map onto the frequency plane as a set of fold singularities. These folds may also be obtained as formal solutions of Eq. (18) or the more complex relation, Eq. (20). Eq. (18) takes a simple form that will be seen later

$$J \propto \Psi(\theta, \phi) = \cos \theta \sin^3 \theta \cos \phi \sin \phi = 0, \quad (33)$$

which gives the same folds obtained from our consideration of the symmetry of the transition frequencies.

The mappings of the folds—the two meridians  $\phi = 0, \phi = \pi/2$  and the equator  $\theta = \pi/2$ —form the boundaries of the HYSCORE line in the frequency plane, which is the mapping of the spherical triangle. The shape of the HYSCORE line is a curvilinear triangle and it is possible to find analytical relations for its boundaries in the frequency plane. The ridges are simple triangles when considered in terms of squares of the two frequencies,  $(\omega_1^2, \omega_2^2)$ , called the  $\omega^2$ -plane for simplicity. For the fold along the equator,  $\cos \theta = 0$ , so that one obtains a parametric form for Eq. (17):

$$\begin{aligned} \omega_1^2 &= c_{j,n}^2 \left[ D_{x,X}^2 + (D_{x,Y}^2 - D_{x,X}^2) \sin^2 \phi \right], \\ \omega_2^2 &= c_{r,s}^2 \left[ D_{\beta,X}^2 + (D_{\beta,Y}^2 - D_{\beta,X}^2) \sin^2 \phi \right], \end{aligned} \quad (34)$$

which is a straight line segment on the  $\omega^2$ -plane connecting the points  $(c_{j,n}^2 D_{x,X}^2, c_{r,s}^2 D_{\beta,X}^2)$  and  $(c_{j,n}^2 D_{x,Y}^2, c_{r,s}^2 D_{\beta,Y}^2)$ . The two other folds also map as straight line segments which connect these two points with the map of the pole at  $(c_{j,n}^2 D_{x,Z}^2, c_{r,s}^2 D_{\beta,Z}^2)$ . Examples of ridges in the absence of NQI are displayed in Fig. 4. The standard frequency plane and the  $\omega^2$ -plane are shown. The only singularities are the folds which outline each of the HYSCORE lines.

The signal intensity is exactly zero when the external magnetic field lies along a principal axis of the hyperfine tensor. This condition occurs at the vertices of each ridge in the HYSCORE spectrum for this nuclear spin Hamiltonian. Thus, the singularities can be prominent on the sides of each HYSCORE line, but must vanish at the vertices. However, the vertices can be easily located by a simple linear extrapolation of the singularity edges in the  $\omega^2$ -plane [5]. The vertices give the frequencies of the principal values of the hfi and therefore completely describe the hfi and the nuclear spin subhamiltonians.

Both single quantum transition frequencies are the same for this nuclear spin Hamiltonian which imparts a characteristic feature to the HYSCORE spectrum that has some utility in the analysis of spectra. The sq-dq and dq-sq ridges have the same form of the sq-sq ridges but are expanded by a factor of two in one dimension, and the dq-dq ridges are expanded in both dimensions. If point  $(\omega_1, \omega_2)$  is observed on a sq-sq singularity on the frequency plane, the following points also lie on singularities and have non-zero spectral density: sq-dq— $(\omega_1, 2\omega_2)$ , dq-sq— $(2\omega_1, \omega_2)$ , dq-dq— $(2\omega_1, 2\omega_2)$ , and due to the symmetry features of the HYSCORE spectra,  $(\omega_2, \omega_1)$ ,  $(\omega_2, 2\omega_1)$ ,  $(2\omega_2, \omega_1)$ ,  $(2\omega_2, 2\omega_1)$ . In addition, all the HYSCORE lineshapes are simple triangles in the  $\omega^2$ -plane.

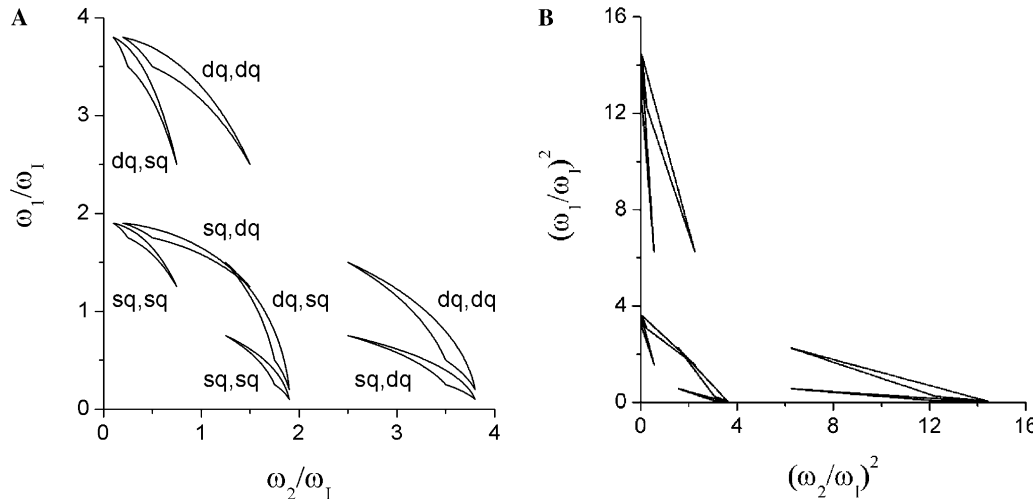


Fig. 4. The singularities of the HYSCORE spectrum in the absence of NQI (A) on the frequency plane, the types of correlation are indicated for each HYSCORE line; and (B) on the  $\omega^2$ -plane. Parameters of the nuclear subhamiltonian were as follows:  $\omega_I = 1$ ,  $A_{X,X} = 1.8$ ,  $A_{Y,Y} = 0.5$ , and  $A_{Z,Z} = 1.5$ .

These results systematically extend our earlier results [5] from  $I = 1/2$  to arbitrary  $I$  in the absence of NQI. We note here that Eq. (28) is quite general for all  $I$  when  $\kappa = 0$ , with  $c_{j,k}$  taking integer values from 1 to  $2I$ , so that all HYSCORE lines, whether involving single or multiple quanta, have the same shape properties as for  $I = 1$  and that the only singularities are the folds outlining each HYSCORE line.

#### 4.1.2. Axial symmetry of the hyperfine interaction

The case of axial symmetry of the hfi tensor introduces additional degeneracies because two principal values of this tensor coincide. This leads to significant simplification of Eq. (31)

$$D_{ms}^2 = D_{ms,\parallel}^2 \cos^2 \theta + D_{ms,\perp}^2 \sin^2 \theta, \quad (35)$$

where  $D_{ms,\parallel}$  and  $D_{ms,\perp}$  are just redefinitions of the quantities given in Eq. (32).

In this situation, the transition frequencies are independent of the azimuth angle  $\phi$ , so that the Jacobian (18) vanishes on the whole sphere

$$J_{\text{axial}}(\kappa = 0) \equiv 0. \quad (36)$$

This means that all HYSCORE lines have zero width, and the triangles in the  $\omega^2$ -plane collapse to straight line segments because two vertexes of triangle coincide (the equator is mapped onto a single point in this case). “General position” is met by every chord connecting the pole and the equator. The ridges become curvilinear segments in the standard frequency plane with delta function cross sections and straight line segments in the  $\omega^2$ -plane which completely describe the hfi [5]. These results hold for all values of  $I \geq 1$  and for crosspeaks of all possible quantum orders.

#### 4.2. Arbitrary NQI

Addition of a quadrupole interaction removes the degeneracy of the single quantum transition frequencies

for nuclear subhamiltonians except in a few very special situations described below. There are potentially 36 ridges in the frequency plane, but some of these ridges may overlap. We do not consider the case of an axially symmetric quadrupolar interaction separately because it is obtained naturally in the limit of small asymmetry.

##### 4.2.1. Isotropic hyperfine interaction

Systems having arbitrary NQI and isotropic hyperfine interaction were considered earlier in detail [16]. It was shown that the HYSCORE lines have zero width, because the effective field affecting the nuclear spin, Eq. (12), is directed along the external magnetic field for both electron spin manifolds. In such a situation, the parameters  $p_{ms}$  (see Eq. (10)) are independent of the PC orientation and the parameters  $q_{ms}$  depend on the same function of orientation,  $f(\eta, \theta, \phi)$ , [15,16] for both manifolds. The immediate consequence is that the Jacobian (18) vanishes

$$J_{\text{iso}}(\kappa \neq 0) \equiv 0. \quad (37)$$

There is no simple way to transform the curvilinear zero width ridges into straight line segments (as could be done in the absence of NQI) or even into simple polynomial or trigonometric functions.

##### 4.2.2. Coincident principal axes for NQI and hfi

When the NQI and hfi principal axes coincide, the quantities  $p_{ms}$  and  $q_{ms}$  in Eqs. (10) and (11) may be arranged in the form of Eq. (31), for example:

$$\begin{aligned} q_{ms} &= q_{ms,X} \sin^2 \theta \cos^2 \phi + q_{ms,Y} \sin^2 \theta \sin^2 \phi + q_{ms,Z} \cos^2 \theta, \\ p_{ms} &= p_{ms,X} \sin^2 \theta \cos^2 \phi + p_{ms,Y} \sin^2 \theta \sin^2 \phi + p_{ms,Z} \cos^2 \theta, \end{aligned} \quad (38)$$

where  $\theta$  and  $\phi$  define the direction of the external magnetic field in the principal axis system of both tensors, and

674

$$\begin{aligned} q_{m_s,U} &= Q_{U,U} \left\{ \omega_I^2 + \frac{1}{4} A_{U,U}^2 + 2m_S \omega_I A_{U,U} \right\} - 2\kappa^3(1-\eta^2), \\ p_{m_s,U} &= - \left[ \omega_I^2 + \frac{1}{4} A_{U,U}^2 + 2m_S \omega_I A_{U,U} + \kappa^2(3+\eta^2) \right]. \end{aligned} \quad (39)$$

676

677 Here  $Q_{U,U}$  are the principal values of the NQI tensor  
678 ( $U = X, Y, Z$ ) given in Eq. (13).

679 The nuclear transition frequencies in this case depend on  
680 the orientation of the external magnetic field in a rather  
681 complex manner, yet they possess the same symmetry features  
682 as described above in the absence of NQI. This means  
683 that the mappings of the four octants of the hemisphere  
684 onto the frequency plane coincide, that “general position”  
685 can be achieved by the same reduction of the unit hemisphere  
686 to an octant, and that Eq. (33) is still valid for the  
687 singularities of the mapping.

688 However, additional singularities are now possible. Eq.  
689 (20) can be factored so that the four components of the  
690 Jacobian may be calculated as the product of two terms:

$$\begin{aligned} J = 4\Psi(\theta, \phi) \times & \left[ \frac{\partial\Omega_\alpha}{\partial p_\alpha} \frac{\partial\Omega_\beta}{\partial p_\beta} \{p_{\alpha,Y}p_{\beta,Z} - p_{\alpha,Z}p_{\beta,Y} + p_{\alpha,Z}p_{\beta,X} \right. \\ & - p_{\alpha,X}p_{\beta,Z} + p_{\alpha,X}p_{\beta,Y} - p_{\alpha,Y}p_{\beta,X}\} + \frac{\partial\Omega_\alpha}{\partial q_\alpha} \frac{\partial\Omega_\beta}{\partial p_\beta} \\ & \times \{q_{\alpha,Y}p_{\beta,Z} - q_{\alpha,Z}p_{\beta,Y} + q_{\alpha,Z}p_{\beta,X} - q_{\alpha,X}p_{\beta,Z} \\ & + q_{\alpha,X}p_{\beta,Y} - q_{\alpha,Y}p_{\beta,X}\} + \frac{\partial\Omega_\alpha}{\partial p_\alpha} \frac{\partial\Omega_\beta}{\partial q_\beta} \{p_{\alpha,Y}q_{\beta,Z} - p_{\alpha,Z}q_{\beta,Y} \\ & + p_{\alpha,Z}q_{\beta,X} - p_{\alpha,X}q_{\beta,Z} + p_{\alpha,X}q_{\beta,Y} - p_{\alpha,Y}q_{\beta,X}\} \\ & \left. + \frac{\partial\Omega_\alpha}{\partial q_\alpha} \frac{\partial\Omega_\beta}{\partial q_\beta} \{q_{\alpha,Y}q_{\beta,Z} - q_{\alpha,Z}q_{\beta,Y} + q_{\alpha,Z}q_{\beta,X} - q_{\alpha,X}q_{\beta,Z} \right. \\ & \left. + q_{\alpha,X}q_{\beta,Y} - q_{\alpha,Y}q_{\beta,X}\} \right]. \end{aligned} \quad (40)$$

693

694 Singularities arise in the mapping (17) if either term in the  
695 product vanishes. The first term on the right hand side is  
696  $\Psi(\theta, \phi)$  from Eq. (33), and results from the symmetry produced  
697 by coincident principal axes. The second factor, in  
698 square brackets, may be rewritten in compact form as

$$\sum_{u,u'=p,q} \frac{\partial\Omega_\alpha}{\partial u_\alpha} \frac{\partial\Omega_\beta}{\partial u'_\beta} (\vec{a} \cdot (\vec{u}_\alpha \times \vec{u}'_\beta)) = 0. \quad (41)$$

701 Here, the auxiliary vectors,  $\vec{p}_{m_s} = (p_{m_s,X}, p_{m_s,Y}, p_{m_s,Z})$ ,  
702  $\vec{q}_{m_s} = (q_{m_s,X}, q_{m_s,Y}, q_{m_s,Z})$ , and  $\vec{a} = (1, 1, 1)$ , are introduced.  
703 Unfortunately, there seems to be no simple way to solve  
704 Eq. (41) except numerically.

705 Fig. 5 displays some examples of the singularities of the  
706 dq, dq HYSCORE line in a frequency spectrum (right-hand  
707 side where the singularities appear as folds or turning  
708 points of the projected surfaces in the frequency plane)  
709 and the respective lines where  $J=0$  on a ‘flattened’ unit  
710 hemisphere (left-hand side) for different values of the quad-  
711 rupole coupling constant. These two displays are comple-  
712 mentary with the frequency display showing the  
713 frequencies of the singularities, but not the corresponding

714 orientations; while the hemisphere display shows the orientations where the singularities occur but not their frequencies. The parameters were chosen to show a range of features in the patterns.

715 The singularities are shown as solid lines in both types of  
716 displays. The patterns look like projections of curvilinear  
717 triangles whose edges are defined by  $\Psi(\theta, \phi) = 0$  in Eq.  
718 (33). These ‘triangles’ may appear twisted and possess additional  
719 singularities if additional folds appear from Eq. (41).  
720 These additional singularities are better resolved on the  
721 surface of the hemisphere than on the frequency plane.  
722 There are two types, the first looks like a bubble connected  
723 to one edge of the octant (Fig. 5D) while the second connects  
724 two different sides of the octant (cases B, E, and F).  
725 These additional folds are too close to the folds from Eq.  
726 (33) to be resolved in the frequency plane.

727 The HYSCORE line in Fig. 5C has a heel-like pattern  
728 on the lower, right-hand side which becomes a narrow  
729 spike in Fig. 5D when the bubble at the equator of the  
730 hemisphere appears. The width of the spike approaches  
731 zero as the bubble approaches the meridian with coordinates  
732  $\theta = \phi = \pi/2$  (where it is highly degenerate, and is  
733 not shown in Fig. 5 because it is not a ‘general position’).  
734 When  $\kappa$  exceeds some critical value ( $\sim 0.61$  for the current  
735 parameters), the pattern becomes like that in Fig. 5E and  
736 looks like a twisted triangle in the frequency plane.

737 Fig. 6 illustrates other features of additional folds in the  
738 frequency plane. In Fig. 6A the distance between the addi-  
739 tional fold (the mapping of a curvilinear segment near the  
740 pole from the left part of Fig. 5B) and the mappings of  
741 both meridians,  $\phi = 0$  and  $\phi = \pi/2$ , are displayed. The  
742 mappings of the meridians cross each other. The triangle  
743 at the right part of Fig. 5B is twisted near its leftmost ver-  
744 tex. The distance does not exceed  $10^{-3} \omega_I$  and will produce  
745 an intense and likely unresolvable peak. Fig. 6B shows the  
746 additional fold in Fig. 5D and the main fold, which is a  
747 mapping of the equator. The distance between these fea-  
748 tures is less than  $10^{-4} \omega_I$ , meaning that the entire surface  
749 area of the bubble on the left-hand side of Fig. 5D is  
750 mapped onto a very narrow strip in the frequency plane,  
751 producing an unresolved region of high spectral density.

752 In the frequency plane, these additional folds resemble  
753 caustics of a system of rays or wave fronts (shown as  
754 dashed lines in the figure), e.g., the right-most edge in  
755 Fig. 5F.

756 There is an important and useful feature of these  
757 HYSCORE patterns that can aid in the interpretation of  
758 spectra. The positions on the hemisphere which are solu-  
759 tions of Eq. (33) depend neither on the transition number  
760 nor on the electron spin manifold when the tensor axes  
761 are coincident. Along the edges of the octants defined by  
762 the coincident principal axes of the NQI and hfi, all three  
763 transitions of each manifold map to fold singularities. If  
764 a vertical (or horizontal) line is drawn through the  
765 HYSCORE spectrum so that it intersects the ridges for  
766 all three nuclear transitions (as shown in Fig. 7), that ver-

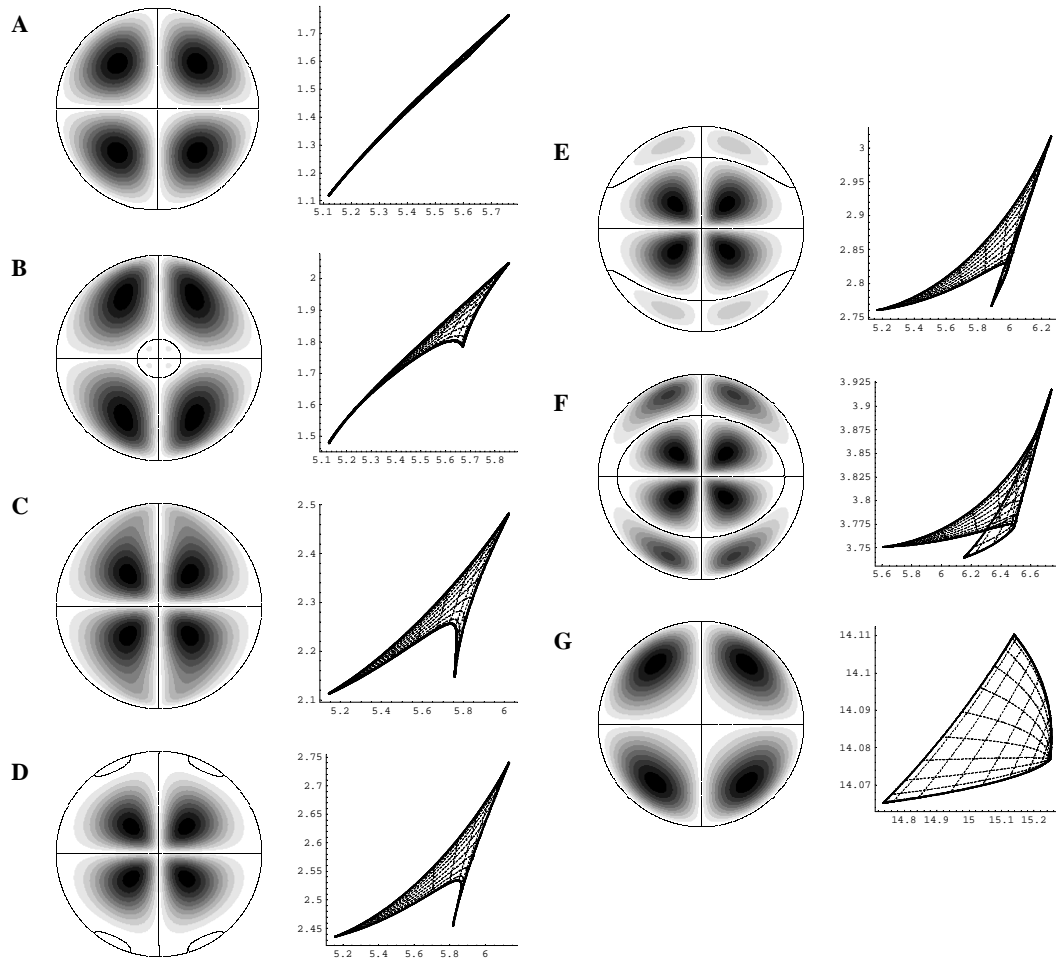


Fig. 5. The value of  $|J|/\sin\theta$  on the hemisphere surface (with solid line drawn for orientations where the Jacobian  $J = 0$ ) (first column) and that of the singularities on the frequency plane of  $dq$ - $dq$  ridge (second column). The radius is proportional to the value of angle  $\theta$ ,  $0 \leq \theta \leq \pi/2$ . The quadrupole coupling constant was varied,  $\kappa = 0.04$  (A),  $0.3$  (B),  $0.5$  (C),  $0.6$  (D),  $0.7$  (E),  $1.0$  (F),  $4.0$  (G), from top to bottom. All other parameters were as follows,  $\omega_I = 1$ ,  $\eta = 0.5$ ,  $A_{X,X} = 3.76$ ,  $A_{Y,Y} = 3.62$ , and  $A_{Z,Z} = 3.12$ .

771 tical line intersects the singularity lines of Eq. (33) at fre-  
772 quencies related by  
773

$$774 \Omega_{ms}^{0,1} = \Omega_{ms}^{1,2} + \Omega_{ms}^{2,0}. \quad (42)$$

775 This general relation is useful for interpreting HYSCORE  
776 ridges and for relating them back to the orientation of  
777 the molecule. The positions of singularities given by the  
778 solutions of Eq. (41) that are not octant edges, do not have  
779 this property because those singularities correspond to dif-  
780 ferent orientations with different sets of frequencies for  
781 each HYSCORE line. The frequencies along the octant  
782 edges can be used to determine elements of Eqs. (38) and  
783 (39).

784 In the case of weak quadrupole interaction, relation (42)  
785 for the singularities is a good approximation even when the  
786 tensor principal axes do not coincide, thus allowing fairly  
787 accurate estimation of the spin Hamiltonian parameters.  
788

#### 789 4.2.3. The absence of any symmetry

790 When the principal axes of NQI and hfi are not collin-  
791 ear, there are no elements of additional symmetry in the

792 nuclear spin Hamiltonian (7) to aid in solving the right-  
793 hand side of Eq. (20) and numerical methods are required.  
794

795 The quantities  $p_{ms}$  and  $q_{ms}$  are defined in terms of the  
796 invariants [16] of the Hamiltonian and depend quadratically  
797 on components of the unit vector  $\vec{k}_z$ . The quantity  $-p_{ms}$   
798 is positively defined which, in principle, allows one to diag-  
799 onalize both terms by the same linear transformation [19].  
800 Unfortunately, this transformation is not a simple rotation  
801 of the coordinate system; a rescaling of the spatial axes is  
802 also required. Consequently, the unit sphere is transformed  
803 into a three-axis ellipsoid in a new system of coordinates.  
804 Moreover, the transformations are different for the each  
805 electron spin manifold, limiting the usefulness of these  
806 transformations in solving the equation  $J = 0$  to find the  
807 singularities.

808 Fortunately, it is not necessary to find the zeroes of Eq.  
809 (40) to locate the singularities in the frequency plane. At  
810 the end of Section 3, we described a method from Catastro-  
811 phe Theory to visualize the singularities simply by project-  
812 ing the parallels and meridians of an arbitrarily oriented  
813 unit hemisphere onto the frequency plane. Fig. 8 shows a

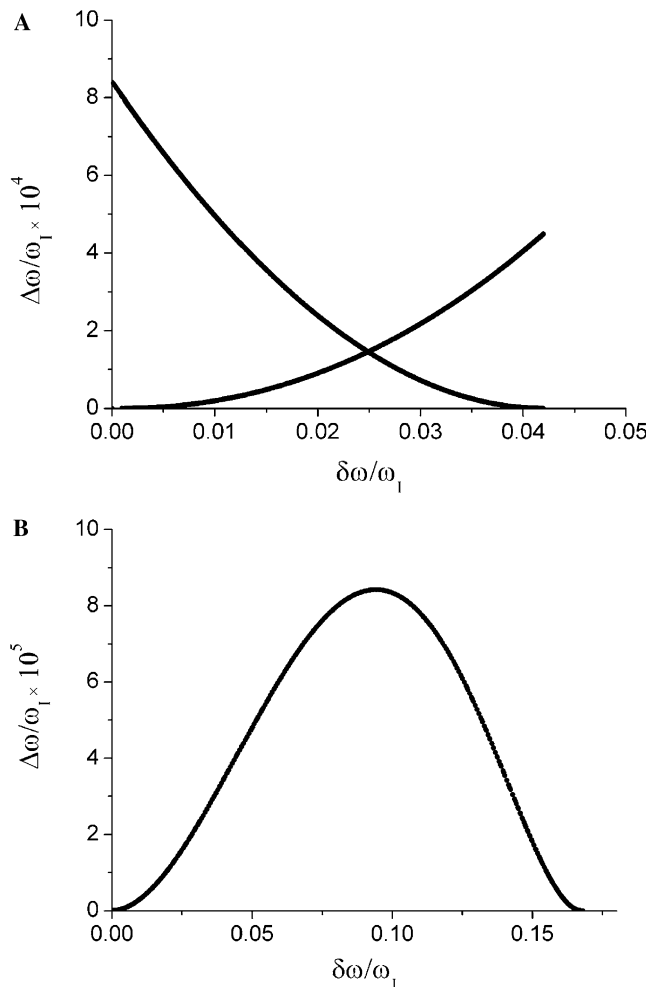


Fig. 6. The distance between additional singularity lines and sides of curvilinear triangles. (A) Additional singularity from Fig. 5B. The distances between mapping of the arc near the pole and mappings of the meridians ( $\phi = 0$  and  $\phi = \pi/2$ ) on the frequency plane ( $\Delta\omega$ ) is plotted versus the distance at the frequency plane between the mappings of the crossing point of the arc and the meridian  $\phi = 0$  and that of the point of the arc ( $\delta\omega$ ). (B) Additional singularity from Fig. 5D. The distance between the mapping of the edge of the ‘bubble’ and the mapping of the equator ( $\Delta\omega$ ) is plotted versus the distance between the mappings of the crossing point of the bubble and equator and the mapping of point of the bubble ( $\delta\omega$ ).

813 set of maps of the parallels and meridians of the unit hemi-  
814 sphere onto the frequency plane illustrating this method.  
815 The folds are easily recognized from the abrupt change in  
816 contrast although the internal cusps are not always appar-  
817 ent when the figures are drawn at low resolution with a lim-  
818 ited number of parallels and meridians.

819 This method of visualizing the singularities is fast and  
820 efficient because it only requires calculating the eigenvalues  
821 for the mapping of Eq. (17) and does not require the inten-  
822 sity coefficients for Eq. (14) or the Jacobian in Eq. (40) or  
823 its roots. It can be useful for rapidly exploring parameter  
824 space of any spin Hamiltonian to find an initial match  
825 between singularities and the prominent features in an  
826 experimental spectrum before investing in more time-con-  
827 suming simulations.

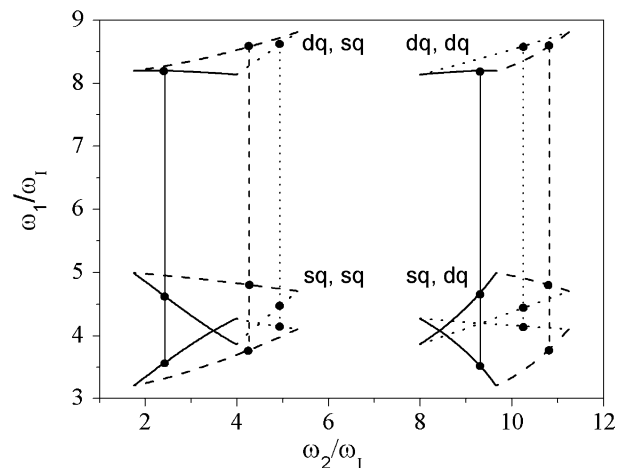


Fig. 7. Example of the additive relation of Eq. (42) between singularities from Eq. (33). Three ridges of  $m_s = -1/2$  manifold correlate the double quantum transition (right ‘column’) and one of the single quantum transitions (left ‘column’) of  $m_s = 1/2$  electron spin manifold. Parameters are as follows,  $\omega_1 = 1$ ,  $\kappa = 2$ ,  $\eta = 0.9$ ,  $A_{X,X} = 6.1$ ,  $A_{Y,Y} = 4.7$ , and  $A_{Z,Z} = -0.3$ . The type of line dashing is the same for the same folds. The vertical lines illustrate that points on the same ‘edge’ (marked by the solid dots) are related by Eq. (42). This relationship can be used to distinguish Eq. (33) singularities from those of Eq. (41) and to identify which singularities correspond to the same ‘edge’.

There are several important characteristics for this case of no symmetry. One is that none of the singularities necessarily correspond to principal values of the hfi or NQI tensors, or even to  $\theta$  or  $\phi$  taking on values of 0 or  $\pi/2$ . Consequently, it can be dangerous to interpret features in the spectrum as principal values. A second characteristic is that the singularities for each HYSCORE line with different  $n_\alpha$  and  $n_\beta$  can occur at different orientations on the unit hemisphere. That is, plots like those on the left-hand side of Fig. 5 can be different for each of the nine ‘unique’ HYSCORE lines. As a consequence, singularities in two different lines generally correspond to two different orientations and the additive relation in Eq. (42) and Fig. 7 will not hold. A final characteristic is that the internal singularities, for a variety of reasons, can be more intense in a spectrum than the fold that outlines the HYSCORE line. As a consequence, the observed features in a spectrum can not be considered as an upper or lower bound for that transition.

## 5. General features of HYSCORE spectra

Every HYSCORE line in spectra from a collection of randomly oriented PCs has certain common features. The most important feature is that the outer edge of each ridge is a singularity line. This property results from the fact that the frequencies are analytic functions of the orientation and are degenerate with respect to inversion of the magnetic field.

This is easily seen in Fig. 8 where the unit hemisphere maps onto the frequency plane as one continuous closed surface. Because the surface has no ‘edges’, the boundaries

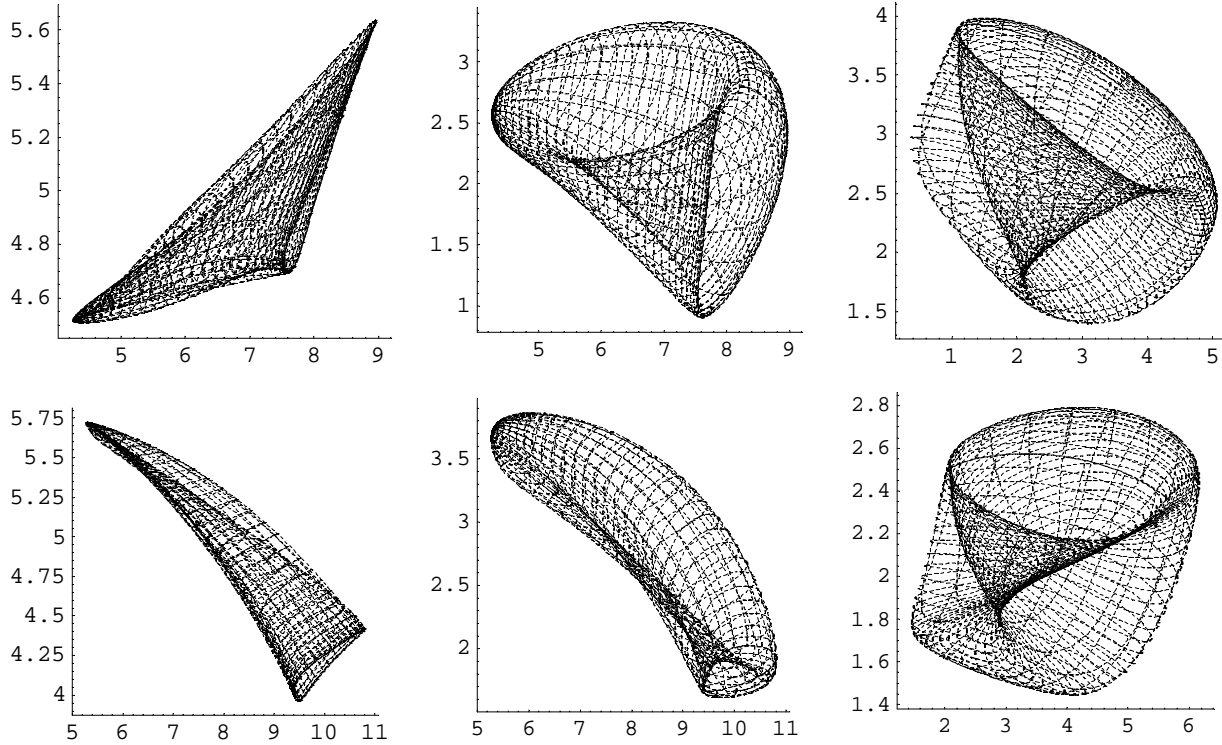


Fig. 8. Fast visualization of the singularity ridges by mapping the parallels and the meridians from the hemisphere onto the frequency plane. Parameter values for the upper row were as follows:  $\omega_I = 1$ ,  $\kappa = 2$ ,  $\eta = 0.9$ ,  $A_{X,X} = 6.1$ ,  $A_{Y,Y} = 4.7$ ,  $A_{Z,Z} = -0.3$ , Euler angles (orientation of the NQI tensor system with respect to the hfi principle axes) were  $50^\circ$ ,  $40^\circ$ , and  $80^\circ$ , for the lower row the nuclear Zeeman frequency was a factor of two larger,  $\omega_I = 2$ . The ridges correlating transitions with  $n_x = n_\beta = 1$  (dq, dq) (the first column);  $n_x = 1$ ,  $n_\beta = 2$  (dq, sq) (the second column); and  $n_x = 2$ ,  $n_\beta = 3$  (sq, sq) (the third column) are displayed. The (dq, dq) transitions for both sets of parameters resemble the ‘glued’ hemisphere in Fig. 3D. Each of the three sides has two crossing folds. Conversely, the (dq, sq) and (sq, sq) lines are bounded by a single fold but have an additional set of internal singularities that appear to be threefold joined at three cusps.

of the HYSCORE line must be a fold and hence a singularity. Consequently, the boundaries or ‘contour lineshape’ [5] is a significant feature of HYSCORE spectra for nuclei with any spin. When the NQI is significant, there may be other singularities on the interior of a HYSCORE line and some care is needed that they are not mistaken for the boundary of the line.

The singularities in HYSCORE spectra are modified by experimental conditions in three ways. (1) The singularities are not infinite in intensity, but become sharp ridges because of the finite range of the observation times  $t_1$  and  $t_2$ , [5], broadening from electron and nuclear spin relaxation and from ‘strain’ or a dispersion in the NQI or hfi parameters. (2) This paper focuses on the singularities caused by mapping. The intensity factors,  $A$  and  $B$ , Eq. (14), can become zero and make a portion of the singularity disappear. Although  $A$  and  $B$  are functions of  $\tau$ , Fig. 1B, there can be regions of the unit hemisphere where  $A$  and  $B$  vanish for all values of  $\tau$ , making some portion of the singularity unobservable. Fig. 9 shows the singularities (or Fourier transform ‘star’ artifacts) and the corresponding calculated HYSCORE contour spectra that take into account the intensity factors. All the major features in the calculated spectra corresponds to singularities. This agreement between spectral features and singularities justifies our focus on the singularities at the expense of the

intensities which also depend on experimental and data processing parameters. (3) An experimental measurement may not include all of the orientations represented by the unit hemisphere. If the paramagnetic centers in the sample are even partially ordered, some regions of the unit hemisphere will not be represented in the measurement and singularities in those un- or under-represented regions will be absent or reduced. In similar fashion, the EPR resonance condition may prevent some orientations of the paramagnetic center from participating in the HYSCORE measurement, a condition known as ‘orientation selection’ and is often the result of large  $g$ -factor anisotropy. The probability,  $P(\theta, \phi)$ , that an orientation contributes to the spectrum enters into the integration over the unit hemisphere to obtain the HYSCORE spectrum in either the time- or frequency-domain. The integral can be rearranged to incorporate  $P$  with the intensity factors  $A$  and  $B$ . It then is possible to write Eq. (14) with  $A'_{njrs}(\theta, \phi) = P(\theta, \phi)A_{njrs}(\theta, \phi)$ , and similarly for the  $B$  term, replacing the original  $A$  and  $B$ . The  $A'$  and  $B'$  are still bounded because the normalized  $P$  are also bounded. Thus, we make the same arguments made earlier that the prominent features in an experimental HYSCORE spectrum will coincide with singularities. However, there may be fewer features because the orientations that give rise to them are absent from the observation.

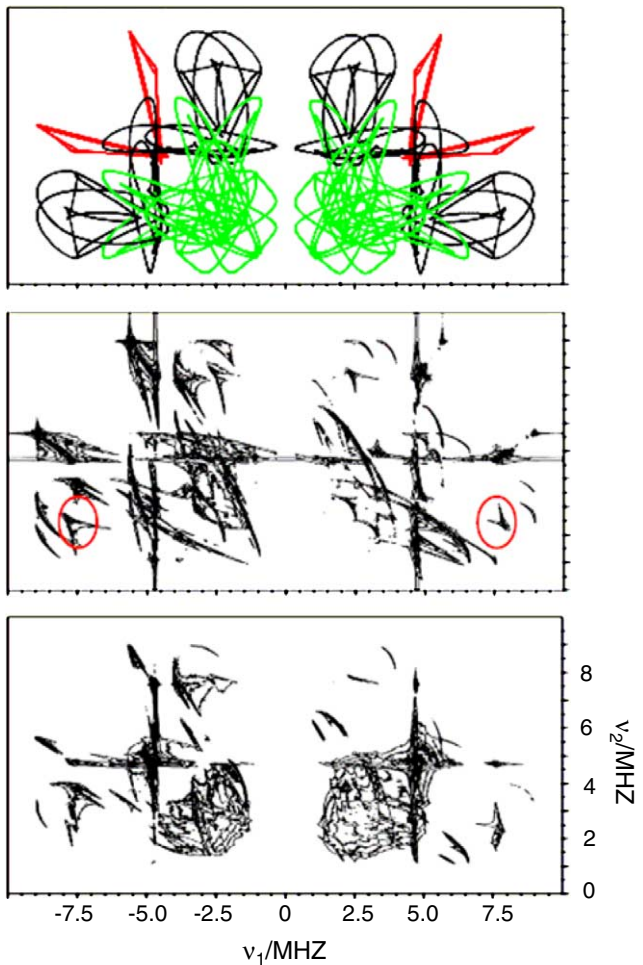


Fig. 9. Singularities for all possible crosspeaks and HYSCORE spectra simulated using the program HYSCORE3 by A.M. Tyryshkin. The upper figure are the singularities: red denotes the dq, dq singularities; black the dq, sq and sq, dq; and green the sq, sq. The middle figure is a simulated spectrum in the limit of small  $\tau$  ( $=10$  ns) and the lower spectrum is simulated with  $\tau = 200$  ns. Spectra were simulated in the time domain from  $t_1 = t_2 = 0$  and processed without apodization. Parameter values are:  $\omega_I = 1$ ,  $\kappa = 2$ ,  $\eta = 0.9$ ,  $A_{X,X} = 6.1$ ,  $A_{Y,Y} = 4.7$ ,  $A_{Z,Z} = -0.3$ , Euler angles (orientation of the NQI tensor system with respect to the hfi principle axes) are  $50^\circ$ ,  $40^\circ$ , and  $80^\circ$  for  $g = 2.0023$  with  $S = 1/2$ ,  $I = 1$ . The red ellipses in the middle figure mark internal fold singularities meeting in cusps for the dq, sq and sq, dq lines. The three figures are plotted to the same frequency scale.

910 The orientational probability,  $P$ , is under some exper-  
911 imental control, for example, by changing the resonance  
912 condition when there is orientation selection or by rotating  
913 the samples when there is partial alignment. There may be  
914 some possibility of extracting information about  $P$  from a  
915 series of HYSCORE spectra, but our interest is focused  
916 on the ability to use the singularities to make a rapid anal-  
917 ysis of hfi and NQI parameters. Even in the presence of  $g$ -  
918 factor anisotropy, it still is feasible to exploit the mapping  
919 singularities with a set of experimental spectra obtained at  
920 several positions in the anisotropic EPR spectrum.

921 The singularities in the HYSCORE lines change  
922 smoothly as the nuclear Zeeman, hfi, and NQI parameters  
923 vary because the transition frequencies of the nuclear sub-

hamiltonian involved in the mapping are analytic functions  
924 of these parameters. Eight dimensionless parameters  
925 describe the nuclear subhamiltonian, which are too many  
926 to study systematically in a single paper. Only one parameter,  
927 the nuclear Zeeman interaction, is an experimental  
928 variable, it depends on the EPR measurement frequency  
929 through the EPR resonance condition. Recent progress in  
930 pulsed EPR instrumentation suggest that it may soon be  
931 possible to make HYSCORE measurements for some  
932 nuclei with EPR frequencies in the range of 0.3–  
933 270 GHz. We show, Fig. 10, a few examples of HYSCORE  
934 lineshapes in this frequency range. We use preliminary hfi  
935 and NQI parameters for one of the nitrogens in the Rieske  
936 iron–sulfur cluster with the tensor axes slightly skewed and  
937 we completely ignore orientation selection. This example  
938 does not correspond to any of the special cases discussed  
939 above and most of the calculated lines contain internal  
940 singularities.  
941

There are three types of HYSCORE lines, each with its  
942 own properties. The dq, dq lines ( $n = j + k = 1$  in Eq. (15))  
943 start at low EPR frequencies as narrow lines, roughly par-  
944 allel to the diagonal of the frequency plane. The dq, dq lines  
945 broaden and then narrow as EPR frequency increases,  
946 becoming narrow ridges roughly perpendicular to the diag-  
947 onal in the high frequency limit. At low frequency, the  
948 transition frequencies for the two transitions are nearly  
949 degenerate, producing a line on the diagonal. At high fre-  
950 quencies, the NQI is a slight perturbation on the dq fre-  
951 quencies and the lineshape converges to that for  
952 vanishing NQI.  
953

For the sq, sq line with  $n = 2$  (or 3) for both frequencies,  
954 the lineshape is again a straight line along the diagonal at  
955 low frequency for the same reason as for the dq, dq transi-  
956 tion. The line broadens with increasing frequency, reaching  
957 a limiting shape when  $\omega_I \gg hfi$  determined by both the hfi  
958 and NQI. This high frequency limit may provide good con-  
959 ditions for complete determination of the spin Hamiltonian  
960 parameters because the shapes approach the ‘first-order’  
961 lineshape.  
962

Lines characterized by different values of  $n$  (the dq, sq  
963 and some sq, sq lines) are generally broad at all frequencies  
964 because the anisotropy of the two transition frequencies  
965 involved are generally quite different for finite NQI. The  
966 strongest changes of the HYSCORE patterns take place  
967 when the nuclear Zeeman frequency has the value close  
968 to the cancellation condition,  $\omega_I = 1/2a$  (K-band for the  
969 parameter set at Fig. 10) [20].  
970

The intensity factors,  $A$  and  $B$ , vary with the inverse  
971 square (or even higher power) of the EPR frequency at  
972 high frequency, placing a practical limit on high frequency  
973 measurements. However, the high sensitivity and first-or-  
974 der lineshapes may make high-frequency measurements  
975 desirable. For finite NQI, the intensities reach a limiting,  
976 generally non-zero, value for low EPR frequencies because  
977 the eigenfunctions in the two electron spin manifolds  
978 become complex conjugates of each other although the  
979 eigenvalues become degenerate [21].  
980

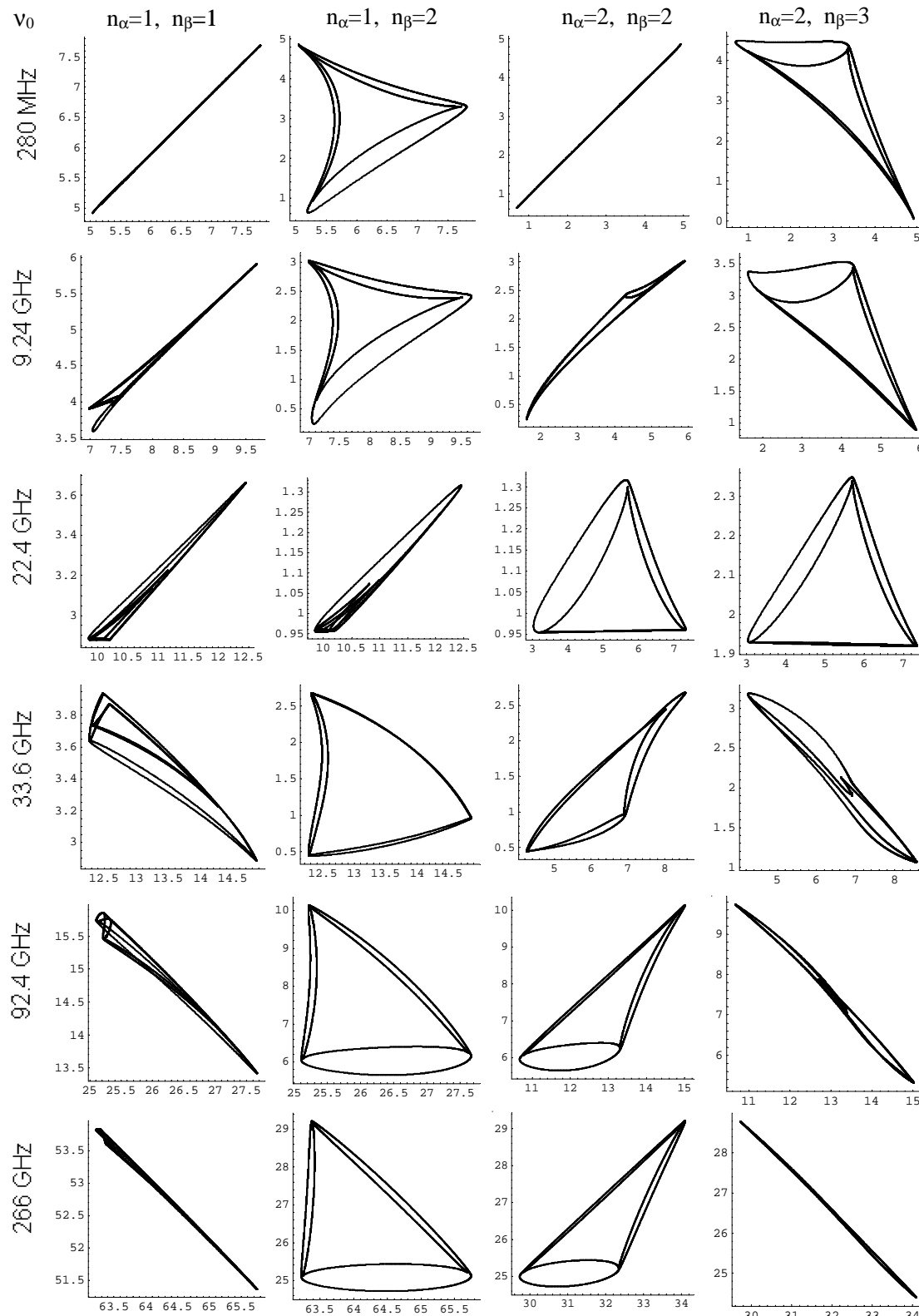


Fig. 10. The example of the transformations of the ridges singularities with variation of the external magnetic field strength for ridges of different types. The types of the ridges are in the column headings. The working frequency of the EPR spectrometer is shown in the leftmost column, the nuclear Zeeman frequency was calculated for  $^{14}\text{N}$  nucleus. The other parameters needed for calculations were as follow,  $\kappa = 0.8 \text{ MHz}$ ,  $\eta = 0.6$ ,  $A_{X,X} = 7.2 \text{ MHz}$ ,  $A_{Y,Y} = 4.7 \text{ MHz}$ ,  $A_{Z,Z} = 4.9 \text{ MHz}$ , Euler angles (orientation of the NQI tensor system with respect to the hfi principle axes) were  $10^\circ$ ,  $15^\circ$ , and  $5^\circ$ .

## 981 6. Conclusions

982 The 2D spectra of disordered systems are, from mathematical point of view, smooth mappings of the hemisphere  
 983 of possible orientations of the external magnetic field with respect to the molecular frame of the PC. The spectrum  
 984 consists of 36 ridges on the upper half of the frequency plane. Catastrophe theory explains the positions of the singularities of such mappings and provides a classification of them. In our case of smooth mapping of one 2D space onto the other there can be only two types of singularities: folds and cusps. The major features in experimental spectra appear to correspond to these singularities, although not every singularity is seen in any single experimental spectrum.

995 The analysis is based on exact solution of the nuclear spin Hamiltonian. Systems with negligible quadrupole interaction have equidistant nuclear eigenvalues for each electron spin manifold and possess additional elements of symmetry. The singularities in this case are mappings of the large arcs connecting the crossing points of the hemisphere with lines directed along the principle axes of the hyperfine interaction tensor. HYSCORE spectra of such systems are curvilinear triangles on the frequency plane and straight line triangles on the  $\omega^2$ -plane. The sides of those triangles in both representations are singularities of the mapping and the only singularities in this case. The number of unique ridges in the spectrum is reduced to 16 because the frequencies of the two single quantum nuclear transitions are degenerate. When the principle axes of NQI and hfi tensors coincide, the system has the same elements of symmetry as in the absence of NQI and the singularity patterns are curvilinear triangles. There is no simple general function that describes these curvilinear segments. The singularities related to the same transition satisfy relation (42), which may be used for verifying of the coincidence of the systems of the principle axes of NQI and hfi tensors. Additional singularities appear for some values of the Hamiltonian parameters. These may be very close to the sides of triangle thus providing quite large spectral densities. The singularity patterns appear at times like a projection of twisted triangles. In all cases, the bounds of the HYSCORE ridges are singularities of the mapping. There may also be internal singularity lines inside each ridge and singularity lines may cross on the frequency plane.

1027 The singularity patterns are strongly dependent on the operating frequency of the pulsed EPR spectrometer. The most significant transformations take place when the nuclear Zeeman frequency becomes approximately equal to the half of the isotropic hyperfine constant (cancellation condition).

1033 Analysis of singularity patterns is simpler and needs less time than calculations of the HYSCORE signal intensities and provides a promising means for preliminary estimations of the spin Hamiltonian parameters.

## Acknowledegments

This work was supported by the National Institutes of Health, GM61904 and partly by Russian Grant for Scientific Schools, 919.2003.3. A.G.M. thanks Battelle Memorial Institute for a Visiting Scientist Fellowship. Part of this work was performed at the WR Wiley Environmental Molecular Sciences Laboratory, a National Scientific User facility sponsored by the Department of Energy's Office of Biological and Environmental Research and located at Pacific Northwest National Laboratory. We thank the referee who pointed out [4] and A.M. Tyryshkin for his simulation program HYSCORE3.

## References

- [1] R.R. Ernst, G. Bodenhausen, A. Wokaun, Principles of Nuclear Magnetic Resonance in One and Two Dimensions, Clarendon Press, Oxford, 1987.
- [2] A. Schweiger, G. Jeschke, Principles of Pulse Electron Paramagnetic Resonance, University Press, Oxford, 2001.
- [3] M. Linder, A. Höhener, R.R. Ernst, Orientation of tensorial interactions determined from two-dimensional NMR powder spectra, *J. Chem. Phys.* 73 (1980) 4959–4970.
- [4] K. Smidt-Rohr, H.W. Spiess, Multidimensional Solid-State NMR and Polymers, Academic Press, London, 1996, Chapter 6.7.3 and Appendix E.
- [5] S.A. Dikanov, M.K. Bowman, Cross-peak lineshape of 2-dimensional ESEEM spectra in disordered  $S=1/2$ ,  $I=1/2$  spin systems, *J. Magn. Reson. A* 116 (1995) 125–128;
- S.A. Dikanov, A.M. Tyryshkin, M.K. Bowman, Intensity of cross-peaks in HYSCORE spectra of  $S = 1/2$ ,  $I = 1/2$  spin systems, *J. Magn. Reson.* 144 (2000) 228–242.
- [6] T. Poston, I. Stewart, Catastrophe Theory and Its Applications, Dover Publications, Mineola, NY, 1996;
- V.I. Arnold, Catastrophe Theory, Springer, Berlin–NY, 1992.
- [7] P. Hofer, A. Grupp, H. Nebenfuhr, M. Mehring, Hyperfine sublevel correlation (hyscore) spectroscopy: a 2D ESR investigation of the squaric acid radical, *Chem. Phys. Lett.* 132 (1986) 279–282.
- [8] B. Epel, D. Goldfarb, Two-dimensional pulsed TRIPLE at 95 GHz, *J. Magn. Reson.* 146 (2000) 196–203.
- [9] D. Goldfarb, B. Epel, H. Zimmermann, G. Jeschke, 2D TRIPLE in orientationally disordered samples—a means to resolve and determine relative orientation of hyperfine tensors, *J. Magn. Reson.* 168 (2004) 75–87.
- [10] D. Goldfarb, V. Kofman, J. Libman, A. Shanzer, R. Rahmatouline, S. Van Doorslaer, A. Schweiger, Double nuclear coherence transfer (DONUT)-HYSCORE: a new tool for the assignment of nuclear frequencies in pulsed EPR experiments, *J. Am. Chem. Soc.* 120 (1998) 7020–7029.
- [11] L. Xiao, M.E. Kellman, Catastrophe map classification of the generalized normal-local transition in Fermi resonance spectra, *J. Chem. Phys.* 93 (1990) 5805–5820.
- [12] C.E. Zaspel, Cusp catastrophe in the ferromagnetic resonance spectrum of a layered ferromagnet, *Phys. Rev. B* 41 (1990) 786–787.
- [13] L.G. Rowan, E.L. Hahn, W.B. Mims, Electron-spin-echo envelope modulation, *Phys. Rev.* 137 (1965) A61–A71.
- [14] S.A. Dikanov, Yu.D. Tsvetkov, Electron Spin Echo Envelope Modulation (ESEEM) Spectroscopy, CRC Press, Boca Raton, 1992.
- [15] G.M. Muha, Exact solution of the NQR  $I = 1$  eigenvalue problem for an arbitrary asymmetry parameter and Zeeman field strength and orientation, *J. Chem. Phys.* 73 (1980) 4139–4140;
- G.M. Muha, The Zeeman effect in  $S = 1$  systems, *J. Magn. Reson.* 49 (1982) 431–443.

16 A.G. Maryasov, M.K. Bowman / Journal of Magnetic Resonance xxx (2005) xxx–xxx

- 1099 [16] A.G. Maryasov, M.K. Bowman, Hyperfine sublevel correlation  
1100 (HYSCORE) spectra for paramagnetic centers with nuclear spin  
1101  $I=1$  having isotropic hyperfine interactions, J. Phys. Chem. B 108  
1102 (2004) 9412–9420.
- 1103 [17] W.B. Mims, Envelope modulation in spin-echo experiments, Phys.  
1104 Rev. B 5 (1972) 2409–2419.
- 1105 [18] H. Whitney, On singularities of mappings of Euclidian spaces, I.  
1106 Mappings of the plane into the plane, Ann. Math. 62 (1955) 374–410.
- [19] J.G. Broida, S.G. Williamson, Comprehensive Introduction to Linear  
Algebra, Addison-Wesley, Reading, MA, 1989.
- [20] R.G. Larsen, G.J. Gerfen, D.J. Singel, The glories of ESEEM:  
measuring electron-nuclear dipolar couplings in orientationally dis-  
ordered solids, Appl. Magn. Reson. 3 (1992) 369–383.
- [21] R.T. Song, P.E. Doan, R.J. Gurbel, B.E. Sturgeon, B.M. Hoffman,  
Non-Kramers ENDOR and ESEEM of the  $S=2$  ferrous ion of  
[Fe(II)EDTA] $^{2-}$ , J. Magn. Reson. 141 (1999) 291–300.

1107  
1108  
1109  
1110  
1111  
1112  
1113  
1114  
1115